Efficient Beam Flattening for Planar-Integrated Magneto-Optical Traps

Chang-Jiang Huang[1,2†], Hong-Chen Liu[1,2†], Liang Chen[1,2], Chuan-Feng Li[1,2,3], Guang-Can Guo[1,2,3], Chang-Ling Zou[1,2,3*], and Guo-Yong Xiang[1,2,3*]

[1]*CAS Key Laboratory of Quantum Information, University of Science and Technology of China, Hefei* 230026*, China*
[2]*CAS Center for Excellence in Quantum Information and Quantum Physics, University of Science and Technology of China, Hefei 230026, China*
[3]*Hefei National Laboratory, University of Science and Technology of China, Hefei 230088, China*

(Received 25 December 2024; accepted manuscript online 17 February 2025)

The planar-integrated magneto-optical trap (PIMOT) offers a promising platform for miniaturizing cold atom systems, but its performance and laser-power efficiency are limited by the typically Gaussian profile of the input laser beam. In this work, we present a simplified and cost-effective beam shaping solution to transform the Gaussian input into a flat-top intensity distribution using a compact system of four spherical lenses. The reshaped light field could potentially enhances PIMOT performance by improving the uniformity of the optical radiation pressure and increasing the trap distance from the chip surface. With this approach, we demonstrate a substantial reduction in the optical power required to trap 2.5×10^5 ^{87}Rb atoms, down to 30% compared to a standard Gaussian beam input. Our results open the door to more efficient and flexible PIMOT systems for quantum sensing, metrology, and atom-based quantum technology.

DOI: 10.1088/0256-307X/42/3/034203 CSTR: 32039.14.0256-307X.42.3.034203

1. Introduction. Laser cooling and trapping techniques have revolutionized atomic physics and quantum science, enabling a wide range of applications.[1–10] However, the size and complexity of conventional magneto-optical traps (MOTs) have posed challenges for developing portable and scalable cold-atom systems. Conventional MOTs are usually large in size and mass, which consist of coils for anti-Helmholtz magnetic field and six laser beams.[11] In recent years, chip-based atom traps have emerged as a promising approach to overcome these limitations, replacing bulky components such as magnetic coils and beam splitters with microfabricated structures.[12–23] The key elements of a compact MOT system include the vacuum chamber,[12–14] laser system,[16,17] magnetic field configuration,[14,15] and on-chip integrated optical components.[18–21] The integration of these elements is beneficial for advanced applications of miniaturized cold-atom systems, also promises further integration with other on-chip optical devices[24–26] and the realization of hybrid quantum platform that combines atoms with other systems.[27–31] Among these directions, significant progress has been achieved with the grating-based MOTs[18] and the planar-integrated MOTs (PIMOT),[15] where a single input laser beam is reshaped by a diffractive optic to generate the light fields necessary for trapping.

While the PIMOT significantly simplifies the optical setup, its performance depends critically on the intensity profile of the incident light. Gaussian beams, although readily available from most lasers, produce non-uniform radiation pressure that requires beam waists of over 10 mm to reach the force balances for atomic region and lead to a small effective trapping volume, in which the incident and diffracted beams from the planar grating chip overlap to provide balanced optical forces, thus resulting in significant power inefficiency and limiting the MOT's performance. This problem is exacerbated by the reflective nature of the grating chip, which demands even higher input power to compensate for losses and maintain balanced radiation pressure. Additionally, the limited working distance between the trapped atom cloud and the chip surface poses another challenge. The radiation pressure balance that determines the trap position is sensitive to the intensity gradients in the incident beam, and for Gaussian beams, this balance is only achieved close to the chip surface, typically within a few mm. Bringing the atoms so close to the surface can lead to losses due to stray fields and surface imperfections, reducing the trap lifetime and overall performance.

Here we introduce a simplified beam shaping method that transforms a Gaussian input laser into a flat-top intensity profile using only four commercial spherical lenses. Our work provides a compact and practical solution for generating uniform intensity over the PIMOT trapping region while maintaining high optical efficiency. It is anticipated that the reshaped incident beam profile improves the balance of radiation pressure forces within the PIMOT, in-

†These authors contributed equally to this work.
*Corresponding author. Email: clzou321@ustc.edu.cn; gyxiang@ustc.edu.cn
© 2025 Chinese Physical Society and IOP Publishing Ltd. All rights, including for text and data mining, AI training, and similar technologies, are reserved.

creasing the distance of the trapped atoms from the chip surface. This opens possibilities for better control of the atom cloud's position and higher laser power efficiencies. Leveraging the flat-top laser profile generated by the refractive beam shaper, we demonstrate trapping of 2.5×10^5 ^{87}Rb atoms at 100 μK using just 30% of the optical power compared to an unshaped Gaussian beam. The substantial reduction in power consumption paves the way for battery-operated portable cold atom devices. Furthermore, the improvement in the PIMOT's performance will benefit cold atom-based quantum sensing and information processing.

2. Theory and Simulation. The PIMOT is a compact cold atom system that relies on the interplay between optical and magnetic forces to confine and cool atoms. As illustrated in Fig. 1(a), the PIMOT employs a grating chip [Fig. 1(b)] and a planar coil chip [Fig. 1(c)] to generate the necessary light fields and magnetic field gradients, respectively. The grating chip uses periodic microstructures to diffract a single circularly-polarized incident beam into three upward propagating beams. Together with the downward incident beam, form the four cooling and trapping beams.[18] The planar coil chip replaces a pair of anti-Helmholtz coils to provide the approximate quadrupole magnetic field. The combination of the light fields and magnetic gradients creates a restoring force that pushes the atoms toward the trap center, while the scattering of near-resonant photons from the red-detuned laser beams leads to cooling via the Doppler effect.

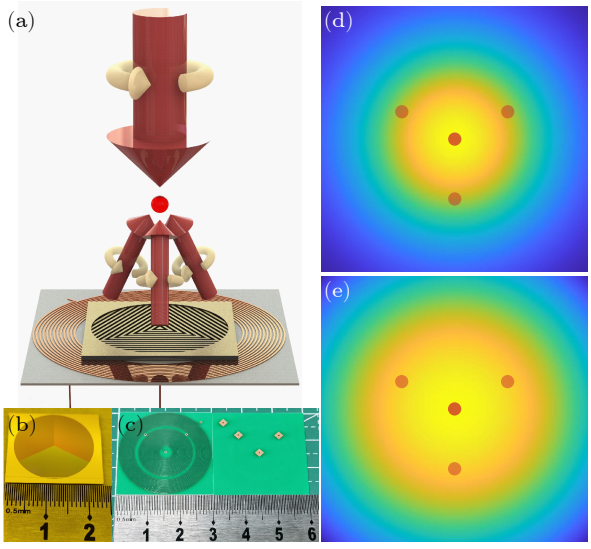

Fig. 1. (a) Schematic of planar-integrated magneto-optical trap. The incident laser beam and three diffraction beams form the light field necessary for trapping the atoms. (b) The grating chip. (c) The planar coil chip. (d)–(e) Different beam waist radii of Gaussian spots correspond to different light intensities in same position.

The optical configuration is a crucial aspect of the PIMOT, as the optical field distribution generated by the single input beam strongly influences the PIMOT's performance. In previous studies,[15] a Gaussian beam is directly emitted from an optical fiber to the grating chip with its center aligned with the chip center. Due to the rotational symmetry, as shown in Fig. 1(d), at a specific radius, the corresponding reflected optical fields can balance with the downward input beam at the center. For a Gaussian beam with limited diameter, the inhomogeneous intensity profile on the grating leads to sharp spatial variation of optical intensities, thus limits the effective trapping volume of the MOT, and the atomic cloud is ellipsoidal rather than spherical.[16]

The intensity distribution of Gaussian light field is

$$I_{\text{in}}(r) = \frac{2}{\pi\sigma_0^2} \times \exp\left[-2\left(\frac{r}{\sigma_0}\right)^2\right], \tag{1}$$

where σ_0 is the radius of the incident beam, and r is the distance from the central axis at the initial plane. Taking $r = 0$ as an example, the downward light field intensity remains constant and is given by

$$I_{\text{down}} = \frac{2}{\pi\sigma_0^2}. \tag{2}$$

The upward light field intensity is influenced by the diffraction angle θ, the diffraction efficiency R, and the corresponding diffraction region of the grating chip. The intensity of a single beam at a height h from the chip surface is given by

$$\begin{aligned} I_{\text{up}} &= R \times I_{\text{in}}\left(\frac{h}{\tan\theta}\right) \\ &= \frac{2R}{\pi\sigma_0^2} \times \exp\left[-2\left(\frac{h}{\sigma_0\tan\theta}\right)^2\right]. \end{aligned} \tag{3}$$

It can be seen that as the Gaussian radius σ_0 increases, the variation in intensity resulting from the change in height h diminishes, indicating a reduced sensitivity of light intensity to height variations and a larger effective trapping volume of MOT. As shown in Fig. 1(e), a larger beam radius leads to a larger distance of the points for balances, and thus the corresponding effective trapping volume increases. It is indicated that a large beam diameter is preferred to maintain a reasonably flat intensity across the trapping region, leading to significant power loss.

To address these issues and enable further miniaturization of the PIMOT, it is essential to employ beam-shaping optics that convert the Gaussian beam into a flat-top profile while preserving high optical efficiency. Our method of reshaping the Gaussian light field is based on the principles of geometric optics.[32] The light rays are redistributed with a lens system, reducing the energy density of the central light field while increasing the energy density at the edges. For simplicity, only the initial and final light fields are considered. The initial light field is same as Eq. (1) and the intensity distribution of the final light field is denoted as I_{out}. Based on the principle of energy conservation, the corresponding relationship between the initial and the final light field on their respective planes can be established

$$\int_0^{r_0} I_{\text{in}}(r) 2\pi r dr = \int_0^{r_0'} I_{\text{out}}\left(r'\right) 2\pi r' dr' = 1, \tag{4}$$

where r_0 is the aperture of the initial light field, and r_0' is the aperture of the final light field. To make the derivation simple, we assume that the energy distribution of the final light field is uniform, meaning the intensity of the light field is

$$I_{\text{out}}\left(r'\right) = \frac{1}{\pi r_0'^2}. \tag{5}$$

Substituting Eq. (1) and Eq. (5) into Eq. (4), we can get

$$\frac{1-\exp\left[-2\left(\frac{r}{\sigma_0}\right)^2\right]}{1-\exp\left[-2\left(\frac{r_0}{\sigma_0}\right)^2\right]} = \frac{\pi r'^2}{\pi r_0'^2}. \tag{6}$$

Based on the derivation above, the designed optical system should ensure that light rays originating from the initial plane at a distance r from the optical axis ultimately exit the system at a distance r' from the optical axis in the final plane. To achieve this, we directly optimize the system using optical simulation software. In practical experiments, the Gaussian light field is emitted directly from a single-mode optical fiber, approximating a point source and the numerical aperture (NA) of the object side is set to 0.11. Actually, only two non-spherical lenses are required to shape the Gaussian light field. However, non-spherical shaping system has issues such as high manufacturing costs and long processing time.

Therefore, we conducted the single spherical shaping system as shown in Fig. 2. The spherical shaping system utilizes four spherical lenses, each consisting of one spherical surface and one flat surface. This design offers a highly practical and straightforward solution that can be readily sourced from Thorlabs or other reputable optical component suppliers. Table 1 presents the key parameters and specifications of the lenses used in the system.

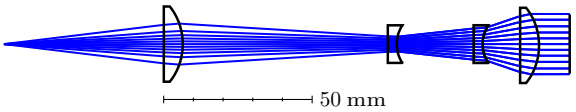

Fig. 2. Schematic of the spherical shaping system, including four lens with $f = 40\,\text{mm}$, $-15\,\text{mm}$, $-30\,\text{mm}$, $35\,\text{mm}$, respectively.

Table 1. The parameters of the spherical shaping system.

Surface	Radius of curvature	Thickness	Glass	Radius
OBJ	infinity	60 (v)		
1	infinity	6.4	H-K9L	12.7
2	−20.6 (v)	54.831 (v)		12.7
3	infinity	3	H-SF11	6.35
4	11.67 (v)	25.408 (v)		6.35
5	infinity	3	H-K9L	6.35
6	15.45 (v)	11.805 (v)		6.35
7	infinity	7.2	H-K9L	12.7
8	−18.03 (v)	10		12.7
IMA	infinity			

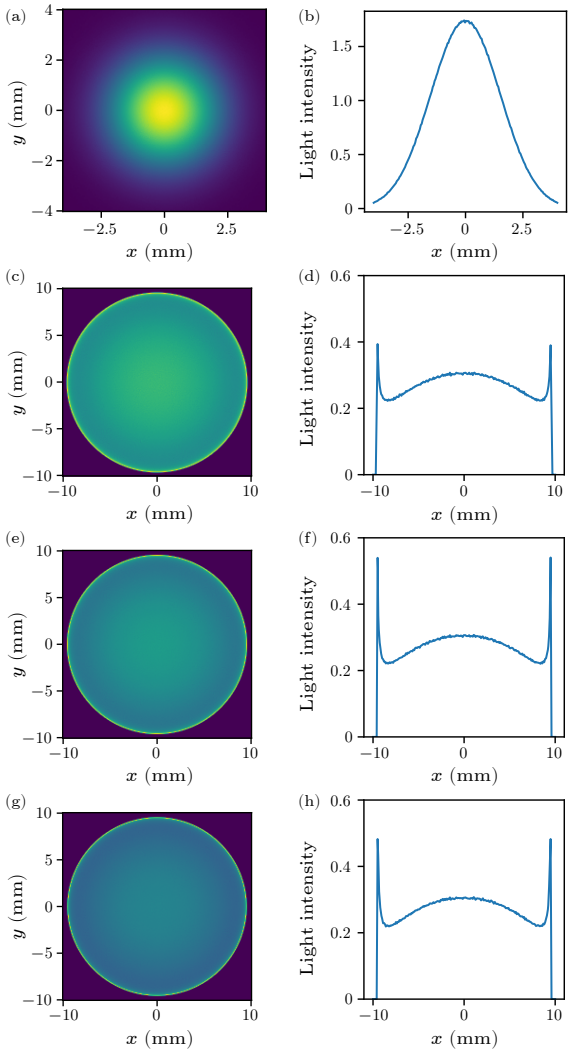

Fig. 3. Simulation diagrams of the spherical shaping system. From top to bottom, they are respectively the Gaussian light field at the first lens, the shaped light field at distances of 10 cm, 20 cm, and 30 cm.

Considering the size and optical field characteristics of the grating chip, we are primarily concerned with the uniformity of the light field within a range of approximately 10 cm to 30 cm after shaping. Thus, we conducted simulations for single spherical shaping system, as shown in Fig. 3. The two-dimensional intensity distribution of the light field and the corresponding intensity distribution along the central are displayed respectively. Figure 3 shows the Gaussian light field at the input surface, followed by the shaped light field at distances of 10 cm, 20 cm, and 30 cm. It can be seen that after passing through the spherical shaping system, the Gaussian light field can cover a circular area with a diameter about 20 mm.

Comparing to the non-spherical shaping system, The uniformity of the single spherical shaping system is not perfect. The sharp protrusions at the edges are due to the limited number of available parameters for the single spherical lens compared to non-spherical lenses. If we restrict the system to spherical lens without considering the matching of commercially available parameters

and simultaneously increase the number of lenses, we can still optimize an excellent light field shaping system same as the non-spherical shaping system. Despite these imperfections, the shaped light field produced by the single spherical system is still a significant improvement over the Gaussian profile for our application with the grating chip.

3. Experimental Results. In the experiment, since the selected lenses are commercially available spherical lenses with diameters of 0.5 or 1 inch, each individually mounted in the cage, we constructed our single spherical shaping system with the cage structure. The spherical shaping system consists of four flat-convex lens with $f = 40\,\text{mm}$, $-15\,\text{mm}$, $-30\,\text{mm}$, $35\,\text{mm}$, respectively. The optical setup is sketched in Fig. 4(a). The shaped light field from the lens passes through a half-wave plate (HWP) to modulate its polarization direction. It then reflects downward from a polarizing beam splitter (PBS) and further undergoes a quarter-wave plate (QWP) to become the left-handed light, serving as the incident field for trapping cold atoms. The planar-integrated MOT configuration uses a grating chip and a planar coil chip, as illustrated in Figs. 1(b)–1(c), which are identical to those used in our previous work.[15]

After passing through the entire shaping and polarization modulation system, the spot diameter is approximately 20 mm. The edge power density is about 90% of the central power density, and the overall divergence is small. Even after propagating approximately 1 m, the diameter changes by less than 2 mm. We captured images of the shaped spot using a CCD camera, as shown in Fig. 4(c). Due to the limited sensor size of the camera, we employed a Galilean scaling system to magnify the spot by approximately 4 times, allowing the camera to capture the entire spot. From Fig. 4(c), we can observe that the shaped light field appears relatively flat. The noise is present due to dust on the lens and the circular diffraction is caused by the limited aperture of the lens. The left and bottom plots in Fig. 4(c) represent intensity profiles along the vertical and horizontal dashed lines, respectively. While there is some fluctuation in the cross-sectional intensity, it remains relatively flat. We also captured images of an unshaped Gaussian light field for comparison in Fig. 4(b). The Gaussian light field exhibits a characteristic central peak with weaker intensity toward the periphery, and its cross-sectional intensity follows a Gaussian distribution, showing significant differences from the shaped light field.

Although the single spherical shaping system has limitations compared to non-spherical systems, it's still better than the simple beam expander using two lens. Moreover, the wasted laser energy is significantly reduced. Using the shaped light field, we successfully trapped the cold atoms with the grating chip. In our experiment, the external-cavity diode lasers are tuned to the 780 nm ^{87}Rb D2 lines. The cooling laser is tuned to the $^5S_{1/2}(F = 2)$ to $^5P_{3/2}(F = 3)$ cycling transition with a detuning of about $-9\,\text{MHz}$, and the repump laser is tuned to the $^5S_{1/2}(F = 1)$ to $^5P_{3/2}(F = 2)$ transition. The incident beam is composed of these two laser beams.

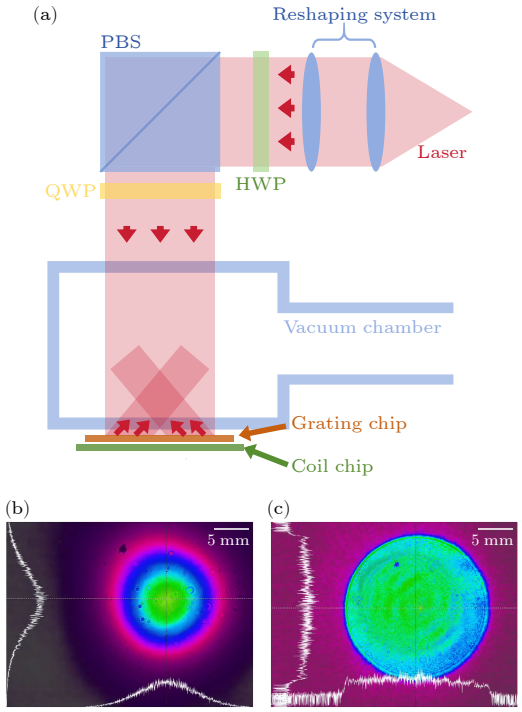

Fig. 4. (a) The spherical shaping system. The laser sequentially passes through the spherical shaping system, HWP, PBS, QWP, and ultimately incidents on the grating chip. (b) The original Gaussian field before the spherical shaping system. (c) The shaped light field after the spherical shaping system.

Compared to the simple collimation system, the single spherical shaping system allowed us to reduce the required laser coupling power from over 100 mW to approximately 30 mW. In both cases, a MOT can be formed and the atoms are polarization gradient cooled (PGC)[33] in 0.5 ms with a detuning $-40\,\text{MHz}$ from resonance. We then measured the temperature and number of the atoms. Figures 5(a) and 5(b) show the fitted squared $1/e$ radius of the atom cloud in the axial (red points) and radial (blue points) directions versus the squared free expansion time t for the previous shaping system with total laser power over 100 mW and spherical shaping system with 30 mW, respectively. The two lines are the fits of $\sigma^2 = \sigma_0^2 + k_\text{B}Tt^2/m$ to the data, where σ is the $1/e$ radius of the atom cloud in the axial (red line) and radial (blue line) directions, k_B is the Boltzmann constant, T is the temperature, and m is the mass of an ^{87}Rb atom.

For previous shaping system with total laser power over 100 mW, the temperature in axial and radial directions can reach 201 μK and 232 μK, respectively. The atom number is $N = 4.2 \times 10^5$ and the density is $\rho = 6.4 \times 10^9\,\text{cm}^{-3}$. Using the spherical shaping system with total power reduced to 30 mW in this work, the temperatures in the two directions were 101 μK and 90 μK, respectively, with an atom number of $N = 2.5 \times 10^5$ and the density is $\rho = 7.2 \times 10^9\,\text{cm}^{-3}$. Photos of cold atoms in the MOT are also shown in Figs. 5(a) and 5(b) with 5 ms exposure time. Comparing the two cases, cold atoms

trapped by the spherical shaping system exhibits greater sphericity, indicating a flatter distribution of the incident laser beam. It can also be seen that the previous shaping system has an atom cloud size of $V = 6.5 \times 10^{-5}\,\mathrm{cm}^3$, while the spherical shaping system has an atom cloud size of $V = 3.5 \times 10^{-5}\,\mathrm{cm}^3$.

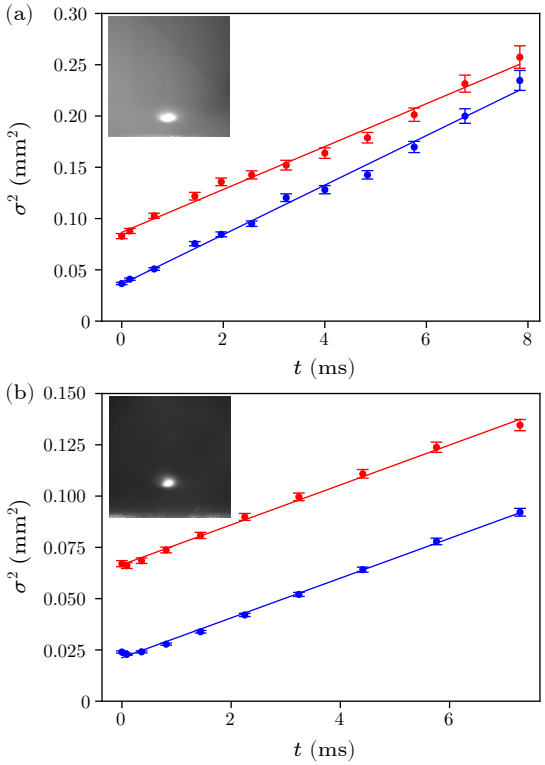

Fig. 5. (a) Temperature and the fluorescence image with previous shaping system. The total laser power is over 100 mW. The temperatures in the two directions are 201 μK and 232 μK, respectively, with an atom number of $N = 4.2 \times 10^5$. (b) Temperature and the fluorescence image with the spherical shaping system. The total power is reduced to 30 mW. The temperatures in the two directions are 101 μK and 90 μK, respectively, with an atom number of $N = 2.5 \times 10^5$.

Comparing the achieved atom density with traditional six-beam MOT, e.g., $\rho = 3.0 \times 10^{10}\,\mathrm{cm}^{-3}$,[34] the PIMOT is limited by the relatively small effective trapping volume. By optimizing the input beam profile, such as using a donut-shaped or other tailored intensity distribution, the effective trapping volume could potentially be expanded while maintaining efficient power usage. Such optimizations could help close the performance gap between PIMOTs and conventional six-beam MOTs while preserving the benefits of the compact planar architecture.

4. Conclusion. In summary, we have demonstrated a simple and effective method for shaping the Gaussian beam in a PIMOT using an all-spherical lens system. By redistributing the light rays according to the principles of geometric optics, the compact four-lens setup transforms the non-uniform Gaussian intensity profile into a flat-top distribution that significantly enhances the performance and efficiency of the PIMOT. Using this spherical shaping system, we have successfully demonstrated trapping of 2.5×10^5 ^{87}Rb atoms at a temperature of 100 μK while reducing the optical power requirement to only 30% compared with a Gaussian input beam. This lays a foundation for reducing the overall power consumption and complexity of chip-based cold atom systems, as well as achieving further miniaturization, for practical applications in sensing, metrology, and quantum technologies.

Acknowledgements. This work was supported by the National Key R&D Program (Grant Nos. 2021YFA1402004 and 2021YFF0603701) and the National Natural Science Foundation of China (Grants Nos. 12134014, U21A20433, U21A6006, and 92265108). This work was also supported by the Fundamental Research Funds for the Central Universities and USTC Research Funds of the Double First-Class Initiative. The numerical calculations in this paper have been done on the supercomputing system in the Supercomputing Center of University of Science and Technology of China. This work was partially carried out at the USTC Center for Micro and Nanoscale Research and Fabrication.

References

[1] Duan L M, Lukin M D, Cirac J I, and Zoller P 2001 *Nature* **414** 413
[2] Matsukevich D and Kuzmich A 2004 *Science* **306** 663
[3] Chou C W, Laurat J, Deng H, Choi K S, De Riedmatten D, Felinto D, and Kimble H J 2007 *Science* **316** 1316
[4] Wang X, Wang J, Ren Z, Wen R, Zou C L, Siviloglou G A, and Chen J 2022 *Phys. Rev. Lett.* **128** 083605
[5] Saffman M, Walker T G, and Mølmer K 2010 *Rev. Mod. Phys.* **82** 2313
[6] Saffman M 2016 *J. Phy. B At. Mol. Opt. Phys.* **49** 202001
[7] Bluvstein D, Evered S J, Geim A A *et al.* 2024 *Nature* **626** 58
[8] Cronin A D, Schmiedmayer J, and Pritchard D E 2009 *Rev. Mod. Phys.* **81** 1051
[9] Ludlow A D, Boyd M M, Ye J, Peik E, and Schmidt P O 2015 *Rev. Mod. Phys.* **87** 637
[10] Wu X, Pagel Z, Malek B S, Nguyen T H, Zi F, Scheirer D S, and Müller H 2019 *Sci. Adv.* **5** eaax0800
[11] Raab E L, Prentiss M, Cable A, Chu S, and Pritchard D E 1987 *Phys. Rev. Lett.* **59** 2631
[12] Burrow O S, Osborn P F, Boughton E, Mirando F, Burt D P, Griffin P F, Arnold A S, and Riis E 2021 *Appl. Phys. Lett.* **119** 124002
[13] Lee J, Ding R, Christensen J *et al.* 2022 *Nat. Commun.* **13** 5131
[14] Yu Z, Zhu Y, Yao M, Qi F, Chen L, Zou C L, Duan J, and Liu X 2024 *Opt. Express* **32** 8919
[15] Chen L, Huang C J, Xu X B *et al.* 2022 *Phys. Rev. Appl.* **17** 034031
[16] McGilligan J P, Griffin P F, Riis E, and Arnold A S 2015 *Opt. Express* **23** 8948
[17] McGehee W R, Zhu W, Barker D S, Westly D, Yulaev A, Klimov N, Agrawal A, Eckel S, Aksyuk V, and McClelland J J 2021 *New J. Phys.* **23** 013021
[18] Nshii C C, Vangeleyn M, Cotter J P, Griffin P F, Hinds E A, Ironside C N, See P, Sinclair A G, Riis E, and Arnold A S 2013 *Nat. Nanotech.* **8** 321
[19] Cotter J P, McGilligan J P, Griffin P F, Rabey I M, Docherty K, Riis E, Arnold A S, and Hinds E A 2016 *Appl. Phys. B* **122** 172

[20] McGilligan J P, Moore K R, Dellis A, Martinez G D, De Clercq E, Griffin P F, Arnold A S, Riis E, Boudot R, and Kitching J 2020 *Appl. Phys. Lett.* **117** 054001
[21] Duan J, Liu X, Zhou Y, Xu X B, Chen L, Zou C L, Zhu Z, Yu Z, Ru N, and Qu J 2022 *Opt. Commun.* **513** 128087
[22] Isichenko A, Chauhan N, Bose D, Wang J, Kunz P D, and Blumenthal D J 2023 *Nat. Commun.* **14** 3080
[23] Blumenthal D J, Isichenko A, and Chauhan N 2024 *Opt. Quantum* **2** 444
[24] Le Kien F, Gupta S D, Balykin V, and Hakuta K 2005 *Phys. Rev. A* **72** 032509
[25] Yalla R, Le Kien F, Morinaga M, and Hakuta K 2012 *Phys. Rev. Lett.* **109** 063602
[26] Barker D S, Norrgard E B, Klimov N N, Fedchak J A, Scherschligt J, and Eckel S 2019 *Phys. Rev. Appl.* **11** 064023
[27] Yang P, Xia X, He H *et al.* 2019 *Phys. Rev. Lett.* **123** 233604
[28] Zhuang W, Zhao Y, Wang S, Fang Z, Fang F, and Li T 2021 *Chin. Opt. Lett.* **19** 030201
[29] Amico L, Anderson D, Boshier M, Brantut J P, Kwek L C, Minguzzi A, and von Klitzing W 2022 *Rev. Mod. Phys.* **94** 041001
[30] Ropp C, Zhu W, Yulaev A *et al.* 2023 *Light: Science & Applications* **12** 83
[31] Yu M, Cheng R, Reimer C *et al.* 2023 *Nat. Photon.* **17** 666
[32] Dickey F M 2018 Laser beam shaping: theory, and techniques (CRC press, 2018)
[33] Dalibard J and Cohen-Tannoudji C 1989 *J. Opt. Soc. Am. B* **6** 2023
[34] Xu L, Wang L X, Chen G J, Chen L, Yang Y H, Xu X B, Liu A, Li C F, Guo G C, Zou C L, and Xiang G Y 2023 *Chin. Phys. Lett.* **40** 093701